Heliyon 10 (2024) e24739

Contents lists available at ScienceDirect

Heliyon

journal homepage: www.cell.com/heliyon

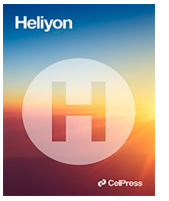

Research article

Impact of inhibitor loaded with pigments content on properties of inorganic zinc rich coatings

Shuangxi Zhou [a], Weijie Li [b], Jianxin Li [a], Ruguang Li [a,*]

[a] Guangzhou Maritime University, China
[b] East China Jiaotong University, China

ARTICLE INFO

Keywords:
Inorganic zinc-rich coating
Corrosion inhibitor
Hydrotalcite
Flake zinc powder

ABSTRACT

In order to overcome the poor dispersion of traditional inorganic zinc-rich coating, addressing the sedimentation and the agglomeration caused by high zinc powder content and improve the anti-corrosion performance of coatings. In this paper, the molybdate intercalated hydrotalcite flake zinc layer double hydroxide ($ZnAl–NO3^-/LDH$) was synthesized by hydrothermal synthesis method at first, and the KH560 modified the Mo/LDH flake zinc powder was further obtained by ion exchange method. The results show that the samples have a layered structure of hydrotalcite with good crystal structure through X-ray diffraction (XRD) and Fourier transform infrared (FT-IR), and the molybdate corrosion inhibiting ions inserted successfully into the interlayer structure of hydrotalcite. Meanwhile, different contents of pigments and fillers were added into the inorganic zinc-rich coatings. It was found that the Nyquist radius of curvature and modulus value of the coating were the largest with a pigment and filler content of 40 %, the maximum corrosion potential was −0.017V, and the minimum corrosion current density was 3.377×10^{-7} A-cm^{-2}. The result indicates that the coating has the best corrosion resistance with 40 % pigment content, which has good application prospects in the fields of cross-sea bridges, natural gas and oil pipelines et al.

1. Introduction

Anti-corrosion coatings are widely used in the field of metal corrosion protection, and the existing market is dominated by inorganic and epoxy anti-corrosion coatings. Compared with epoxy anti-corrosion coatings, inorganic anti-corrosion coatings have low VOC emissions, which conform with the development trend of environment-friendly coatings. Among them, as a representative of inorganic anticorrosive coatings, inorganic zinc-rich coatings have excellent conductivity, solubility, heat resistance and corrosion resistance used silicate as the film-forming base material, zinc powder as the pigment, and a small number of organic substances as additives or auxiliary solvents [1]. However, the conventional inorganic zinc-rich coatings are prone to sedimentation and agglomeration due to excessive zinc powder content, poor dispersion and other shortcomings, which leads to the formation of coating defects and the anti-corrosion effect of the coating, thus greatly reducing the service life of the coating. In order to address the above shortcomings, Sun G et al. [2–9] added corrosion inhibitors to the coating to achieve the self-repairing anti-corrosion function of the coating on the damaged area. The principle is that corrosion inhibitors achieve the anti-corrosion by blocking the dissolution of the anode metal into the water or inhibiting the chemical reaction of the cathode to reduce the electrochemical reaction rate of the metal.

* Corresponding author.
E-mail address: liruguang2005@163.com (R. Li).

https://doi.org/10.1016/j.heliyon.2024.e24739
Received 8 September 2023; Received in revised form 7 January 2024; Accepted 12 January 2024
Available online 16 January 2024

The corrosion inhibiting ions are loaded into the nanocontainer and doped into the coating with the silicate base material. When the corrosive medium began to penetrate, the nanocontainer gradually released the corrosion inhibiting ions into the internal and external solutions of the coating. Combing with the metal cations to generate insoluble metal complexes deposited on the coating surface, which effectively enhances the physical shielding effect of the coating. Liu [10] adopted co-precipitation method to load MoO_4^{2-} into the inter-layer structure of hydrotalcite, and a comparative study by electrochemical impedance technology found that the corrosion resistance of the coating with hydrotalcite filler was stronger than that of the coating without hydrotalcite filler. Yu [11] used a one-step precipitation method to load MoO_4^{2-} into hydrotalcite nanocontainers, and the synthesized Zn/Al–MoO_4^{2-} hydrotalcite nanocontainers could exchange and adsorb different degrees depending on the chloride ion concentration. Then it as a pigment was added into 3.5 % NaCl solution for a period of time, the alternating-current (AC) impedance test of the coating showed that it still had good anti-corrosion performance. The above studies illustrate that corrosion inhibitors can play a role in corrosion protection at coating defects, delaying the diffusion of corrosive ions and improving the barrier and anti-corrosion performance of the coating. Inspired by the above research, hydrotalcite material has excellent adsorption and ion exchangeability. Loading corrosion inhibitors through the interlayer structure of hydrotalcite, the porosity of the coating can be reduced, the diffusion resistance of corrosive media such as water, oxygen, and chloride ions in the coating can be increased, and the mechanical properties of the coating film can be improved.

At present, many scholars have conducted a large number of research on corrosion inhibitors added directly as pigments or loaded into epoxy coatings through carrier materials, but there are few studies have been conducted on the effect of the content of corrosion inhibitors loaded with pigments and fillers on the performance of inorganic zinc rich coatings. In order to improve the anti-corrosion performance of inorganic Zn-rich coatings, ZnAl–NO_3^-/LDH was synthesized in situ on the surface of flake zinc powder by hydrothermal synthesis, and then Mo/LDH flake zinc powder was prepared by the ion exchange method, and its structure was characterized by XRD and FT-IR, and the dispersion of flake zinc powder in the coating was improved by silane coupling agent KH560 modification. Finally, the effect of the change of pigment content on the coating performance was investigated by changing the content of pigments and fillers and using the test methods of adhesion, pencil hardness and electrochemical workstation.

2. Experiment

2.1. Methodology

(1) The preparation of high modulus modified potassium silicate solution: The silica sol with a solid content of 26.15 % was poured into a three-necked flask under the condition of constant temperature water bath at 50 °C. Meanwhile, potassium hydroxide and deionized water were added slowly, and the stirring was continued for about 15 min to obtain a light blue transparent potassium silicate solution with a modulus of 5.5. The freshly prepared potassium silicate solution was measured and poured into the flask under the condition of constant temperature water bath, and 25 % silicone emulsion was slowly added in the state of stirring for about 1 h to obtain the high modulus potassium silicate solution modified by silicone-acrylic emulsion.

(2) The molybdate intercalated hydrotalcite flake zinc powder: 20 g flake zinc powder was added in a 100 mL beaker, washed with deionized water and anhydrous ethanol by ultrasonic, and the washed flake zinc powder was transferred to 200 mL hydrothermal reactor. And then 1.87 g of $CO(NH_2)_2$ and 1.80 g of Al $(NO_3)_3 \cdot 9H_2O$ were dissolved in 100 mL deionized water and transferred to the hydrothermal reactor. The reactor was sealed after filling with nitrogen for 2 min and placed in a blast drying oven at 120 °C for 10 h. After natural cooling, the filter cake was washed with deionized water to neutral and dried to obtain the flake zinc powder loaded with ZnAl–NO_3^-/LDH. In the beaker, 20 g ZnAl–NO_3^-/LDH flake zinc powder was weighed, 500 mL deionized water and 9.88 g $Na_2MoO_4 \cdot 2H_2O$ were added, and the pH was adjusted to 9.5–10 by ammonia. The solution was magnetically stirred at room temperature for 24 h, washed until the solution was neutral, and dried to obtain molybdate intercalated hydrotalcite flake zinc powder (hereinafter referred to as Mo/LDH flake zinc powder).

(3) The modification of Mo/LDH flake zinc powder by silane coupling agent KH560: Firstly, 50 mL isopropanol was poured into the flask, and then a certain amount of Mo/LDH flake zinc powder was added. Finally, 8 % mass fraction of silane coupling agent KH560 was added, stirred for 1 h under constant temperature water bath conditions at 70 °C and washed with ethanol, dried and ground to obtain modified Mo/LDH flake zinc powder.

(4) The preparation of inorganic zinc-rich coating: High modulus modified potassium silicate solution was used as the substrate; modified Mo/LDH flake zinc powder was used as the pigment filler. Different proportions of pigments (mass fraction of 20 %, 30 %, 40 % and 50 %) and small amounts of tributyl phosphate, Tween 20 and sodium polyacrylate were added according to the experimental scheme, and the coatings were obtained after stirring for 15 min.

2.2. Detection and characterization

(1) XRD. The light source is Cu-Kα target radiation, the scanning speed is 10°/min, the scanning range is 5–80°, the voltage is 40 KV, and the current is 30 mA.

(2) Infrared spectral analysis. The scanning speed is 4 cm^{-1}, the number of scans is 32 times, and the test wave number range is 400-4000 cm^{-1}.

(3) Adhesion. A special single-edged tool was used to draw 6 straight lines in the horizontal and vertical directions of the coating surface. The spacing between the straight lines is 1 mm, and after getting a cross grid pattern, the soft bristle brush is repeatedly brushed for 10 times along the diagonal direction of the grid.

(4) Hardness. The testing method is to place the coating sample on a horizontal table and fix it under the conditions of temperature 23 ± 2 °C and relative humidity 50 ± 5 %, and the QHQ-A pencil hardness tester is used for detection.
(5) Powder removal. The surface of the coating is repeatedly wiped for 10 times with vulcanized rubber, and the wiping strength is consistent. And then the surface of the coating was observed to rate the powder removal.
(6) Salt water resistance time. Two-thirds of the samples are immersed in 3.5 wt% NaCl solution, and the coating samples are observed daily for blistering, wrinkling, rusting, and shedding.
(7) Heat resistance. Before testing, the sample should be adjusted at room temperature for 24 h, then baked in the oven for 10 h. After being taken out and cooled, it is compared with other samples at room temperature to observe whether there are changes on the surface of the coating. In this way, whether the heat resistance of the coating meets the standard can be determined.
(8) Electrochemical test. Three-electrode working system, inorganic zinc-rich coating as working electrode, auxiliary electrode as platinum electrode, and reference electrode as saturated glycerol electrode. The signal value is a sine wave with an amplitude of 5 mV, the measurement frequency range is 10^5–10^{-2} Hz, and the voltage scanning rate is 1 mV/s.

3. Results and discussion

3.1. Characterization of Mo/LDH flake zinc powder

Fig. 1 shows the XRD pattern of Mo/LDH flake zinc powder. It can be seen that the characteristic diffraction peaks of (003), (006) and (009) crystal planes reflecting the layered structure of LDH appear when 2θ equals to 11.27°, 23.13° and 31.96° respectively, which reflects the obvious layered structure of LDH and good crystal structure in the synthesized Mo/LDH flake zinc powder. The (003) crystal plane spacing d is calculated as 0.785 nm according to the Bragg Equation $\lambda = 2d\sin\theta$, which is larger compared with the (003) crystal plane spacing d = 0.770 nm of ZnAl–NO_3^-/LDH [12], and the crystal plane angle is deflected to a lower angle, indicating that the pore channel of hydrotalcite becomes larger, which is caused by MoO_4^{2-} intercalation. To sum up, this method can synthesize LDH-Mo with good crystal structure on the surface of flake zinc powder.

Fig. 2 shows the infrared analysis spectrum of Mo/LDH flake zinc powder. As shown, the 3429 cm^{-1} is the characteristic absorption peak of hydroxyl group of water molecules on the surface and inner layer of hydrotalcite, which belongs to the telescopic vibration of H–*O*–H of inter-layer water molecules and the symmetric contraction of hydroxyl group O–H, which is due to the adsorption of water on the surface of the particles and the insertion of a considerable number of H_2O molecules into the inter-layer space [13]. The bending vibration absorption peak of water of crystallization (-OH) appears near 1639 cm^{-1}. The peak of 855 cm^{-1} is the absorption peak of the anti-symmetric stretching vibration of Mo–*O*–Mo in molybdate ions, which indicates that molybdate has been present in the inner layer of hydrotalcite [14]. The absorption peak near 552 cm^{-1} is attributed to the vibration absorption peak of lattice oxygen in the layer, and the absorption peak near 424 cm^{-1} is a typical bending vibration of Zn–Al–OH.

3.2. Influence of corrosion inhibitor content on the basic properties of inorganic zinc rich coatings loaded with pigments and fillers

When pigment fillers loaded with corrosion inhibitors are added to inorganic zinc-rich coatings, their content has an important effect on the coating properties. Table 1 shows the effect of adding different amounts of pigments on the basic properties of the coatings. The experimental results show that the coating surface with a pigment content of 20 % undergoes rusting on the 23rd day, and the time of rusting on the surface of the coating is significantly prolonged with the pigment content, and when the pigment content exceeds 50 %, the excessive pigment content will cause a relative shortage of the substrate, resulting in the failure of bonding between

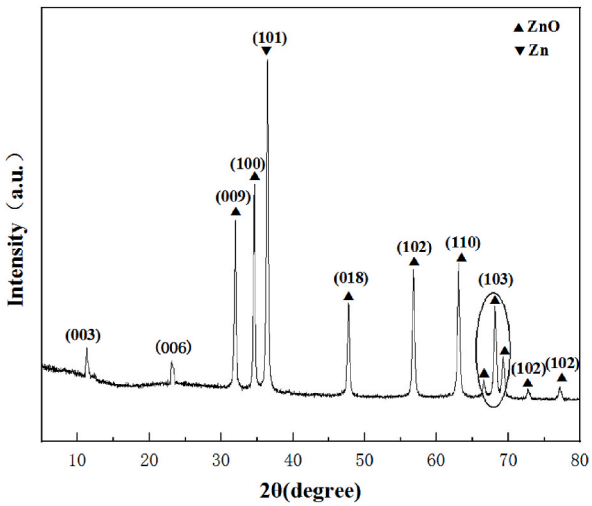

Fig. 1. XRD spectrum of Mo/LDH flake zinc powder.

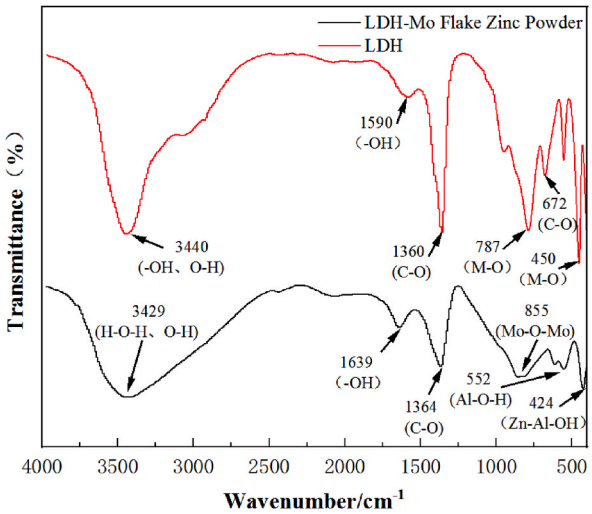

Fig. 2. Infrared analysis spectrum of Mo/LDH flake zinc powder.

Table 1
Basic properties of the coating.

Pigment content/mass%	Adhesion	Pencil hardness	Powder removal	Salt water resistance time/d	Heat resistance (200 °C)
20	2	6H	Level 1	23	intact
30	2	6H	Level 1	> 25	intact
40	2	6H	Level 1	> 25	intact
50	2	6H	Level 1	> 25	intact
60	3	6H	Level 2	21	intact

the pigment and the substrate to form an effective protective film. The adhesion and powder removal of the coating decrease, and the rusting and peeling phenomenon occur on the surface of the coating on the 21st day. It can be seen from the above test results that the coatings with pigment content of 30 %, 40 % and 50 % present the optimal comprehensive performance, and the coatings have better adhesion, hardness, powder removal and salt water resistance time, which can continuously resist high temperature of 200 °C.

3.3. Corrosion resistance of coatings

(1) Electrochemical impedance spectroscopy of the coating

Electrochemical impedance spectroscopy was performed on four coatings with different pigment contents. The magnitude of Nyquist curvature radius and the modal value |Z| reflects the corrosion resistance of the coating, and the time constant of the reaction can be determined from the corresponding phase angle diagram, from which the corrosion stage reached by the coating can be determined. Fig. 3 shows the (a) Nyquist plots and fitting results, (b) Bode plots and (c) Phase-frequency curves of coatings with different pigment content immersed in 3.5 % NaCl solution for 24 h. It can be seen from that the curvature radius and low-frequency modulus of the coating with a content of 40 % are the largest compared with those of the coatings with 20 %, 30 % and 50 % content. There is only one time constant for each coating, indicating that corrosion has not yet occurred on the coating surface at the beginning of immersion, and the coating is in the pre-corrosion stage. And the corrosive medium is isolated by the rod-like ZnO and lamellar LDH structures on the coating surface before penetrating into the coating interior. In addition, the corrosive chloride ions and water molecules will be adsorbed by the molybdate ions loaded between the layers of hydrotalcite during diffusion, slowing down the diffusion of chloride ions and water molecules into the interior of the coating. In order to better explain the corrosion behavior of coatings with different contents soaked in NaCl solution for the same time, the Zview commercial software was used to fit the Nyquist spectrum, and the equivalent circuit diagram was obtained as shown in Fig. 3. In this equivalent circuit diagram (Fig. 4), Rs represents solution resistance, Rp represents passivating film resistance, Rct represents charge transfer resistance at the interface between coating and substrate, CPE-c represents coating capacitance, CPE-ct represents the capacitance between layers of coating, respectively. The values of each parameter in the equivalent circuit diagram are shown in Table 2. Generally, the larger of the Rp, the more difficult the electrochemical reaction is to carry out. It can be seen that with the increase of content, the passivating film resistance first increases and then decreases, and the passivating film resistance is the largest at 40 % content, indicating that the corrosion resistance of 40 % coating is better than that of other content, and can effectively reduce the erosion of corrosive media on the matrix material, which is consistent with the results of the polarization curve.

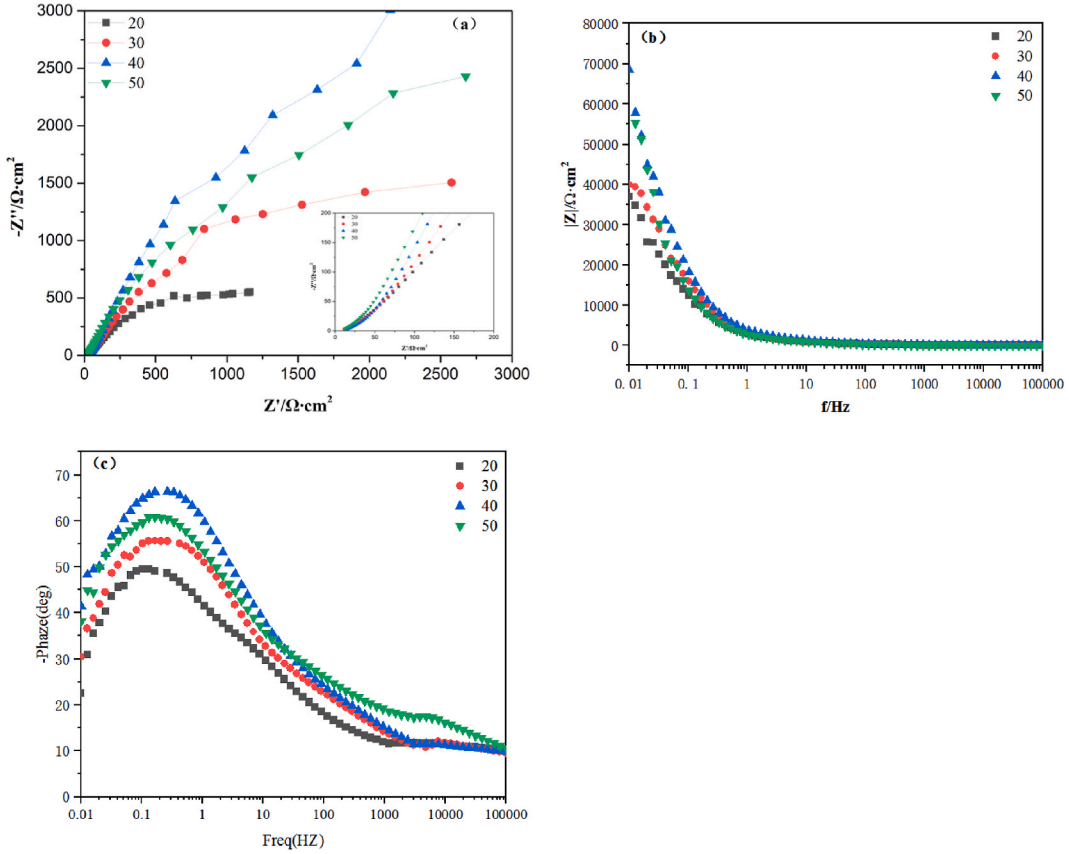

Fig. 3. (a) Nyquist plots and fitting results, (b) Bode plots and (c) Phase-frequency curves of coatings with different pigment content immersed in 3.5 % NaCl solution for 24 h.

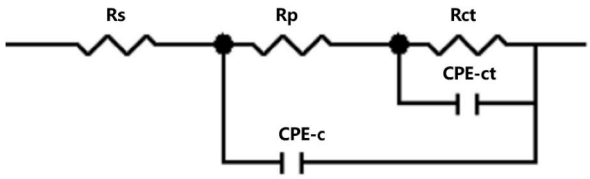

Fig. 4. Equivalent circuit diagram of EIS curves.

Table 2
Fitted results for EIS curves at 24 h in 3.5 wt% NaCl.

Content	R_s/Ω	CPE-c/(S·sn1)	Rp/Ω	CPE-ct/(S·sn2)	Rct/Ω
20 %	14.65	0.00039114	2391	0.57481	13.03
30 %	13.15	0.00031286	23,634	0.60006	12.77
40 %	17.63	0.00021129	9.069E+10	0.66821	16.85
50 %	13.88	0.00023605	44,113	0.65015	13.28

Fig. 5 shows the (a) Nyquist plots and fitting results, (b) Bode plots and (c) Phase-frequency curves of coatings with different pigment content immersed in 3.5 % NaCl solution for 240 h. It can be seen that the Nyquist diagrams of the coatings with different contents show a single incomplete capacitive resistance arc, and the capacitive resistance arc at 240 h is greater than that at 24 h. The possible reason is that the nano-scale flake Zn/Al–MoO_4^{2-} powder shows excellent retardation and corrosion resistance to corrosive media [15]. When the corrosion ions diffuse to the interface between the coating and the metal substrate, the chloride ions are exchanged with the molybdate ions to prevent the chloride ion from diffusing to the substrate. With the increase of pigment content, more MoO_4^{2-} is exchanged, preventing more chloride ions from diffusing to the substrate. Therefore, the coating with large pigment

content has a larger capacitive arc than the coating with small pigment content, indicating that the addition of pigment content will make the corrosion resistance of the coating more significant. In addition, the modulus value of each coating also has a certain increase, which is because with the prolongation of corrosion time, the MoO_4^{2-} loaded between the hydrotalcite layers is slowly released in response to the stimulation of chloride ions, and reacts with the ions in the solution to generate complexes deposited on the surface of the coating or the void, blocking the channel of corrosive medium diffusion through the pores of the coating, playing the role of sealing and self-healing, improving the compactness of the coating and preventing the expansion of the corrosion area. Moreover, molybdate ions undergo adsorption and ion exchange reactions with chloride ions penetrating into the coating, reducing the amount of chloride ions penetrating into the interface between the coating and the substrate metal, alleviating the corrosion of zinc nano-particles in the coating, which can effectively prevent further corrosion of the coating, and improve the electrochemical protection and overall anti-corrosion performance of the coating to a certain extent. In the phase angle diagram, two-time constants appear for each coating, indicating that the coating is in the middle stage of corrosion, which may be due to the diffusion of corrosion ions into the coating began to corrode the Zn nanoparticles, resulting in the appearance of the second time constant. In order to better explain the corrosion behavior of coatings with different contents soaked in NaCl solution for the same time, the Zview commercial software was used to fit the Nyquist spectrum, and the equivalent circuit diagram was obtained as shown in Fig. 5. In this equivalent circuit diagram (Fig. 4), Rs represents solution resistance, Rp represents passivating film resistance, Rct represents charge transfer resistance at the interface between coating and substrate, CPE-c represents coating capacitance, CPE-ct represents the capacitance between layers of coating, respectively. The values of each parameter in the equivalent circuit diagram are shown in Table 3. Generally, the larger of the Rp, the more difficult the electrochemical reaction is to carry out. It can be seen that with the increase of content, the passivating film resistance first increases and then decreases, and the passivating film resistance is the largest at 40 % content, indicating that the corrosion resistance of 40 % coating is better than that of other content, and can effectively reduce the erosion of corrosive media on the matrix material, which is consistent with the results of the polarization curve.

Fig. 6 shows the (a) Nyquist plots and fitting results, (b) Bode plots and (c) Phase-frequency curves of coatings with different pigment content immersed in 3.5 % NaCl solution for 504 h. It can be seen that the curvature radius and low-frequency impedance of each content coating gradually decrease, indicating that the anti-permeation ability of the coating has decreased. The reason for the decline may be that the corrosion ions have been diffused to the substrate, and the hydrotalcite shielding effect has been weakened. With the extension of the immersion time, the continuous penetration of corrosion ions into the coating, and the electrochemical corrosion reaction occurs at the metal interface between the coating and the substrate, leading to a decrease in the barrier performance

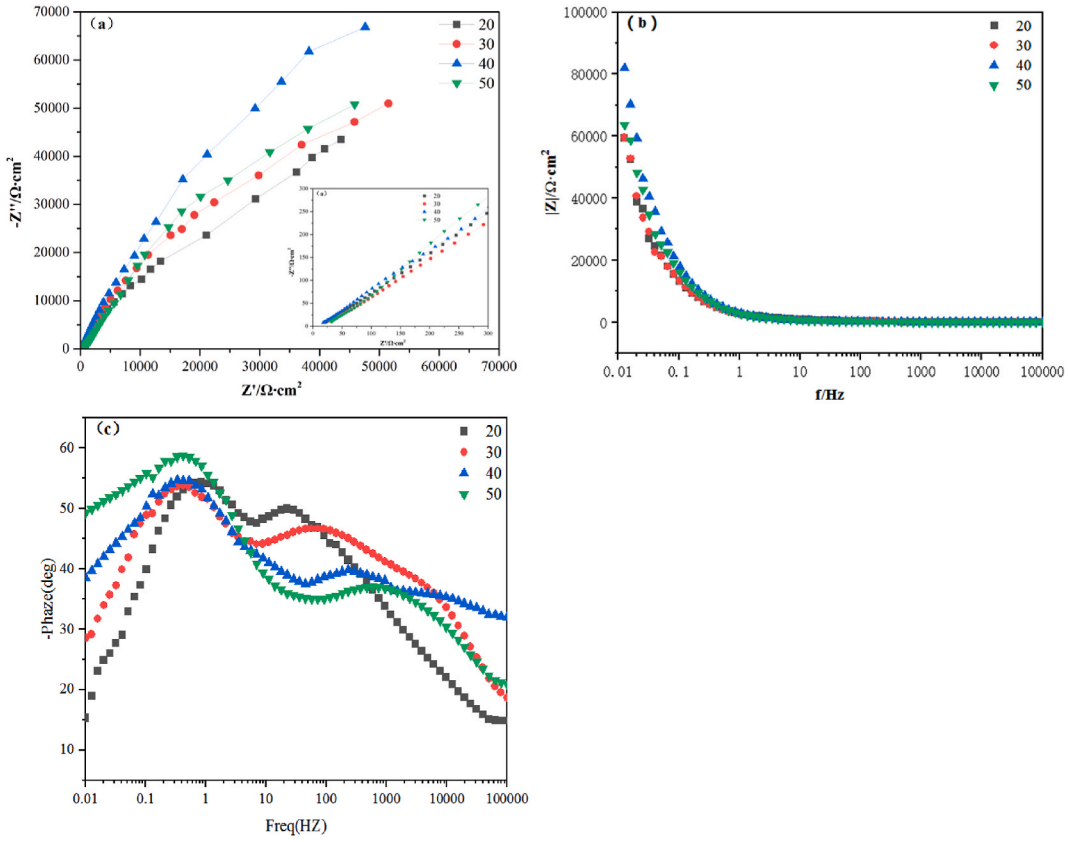

Fig. 5. (a) Nyquist plots and fitting results, (b) Bode plots and (c) Phase-frequency curves of coatings with different pigment content immersed in 3.5 % NaCl solution for 240 h.

Table 3
Fitted results for EIS curves at 240 h in 3.5 wt% NaCl.

Content	R_s/Ω	CPE-c/(S·sn1)	Rp/Ω	CPE-ct/(S·sn2)	Rct/Ω
20 %	18.91	0.00015545	1.028E+12	0.51137	18.76
30 %	29.06	0.00013196	3.585E+11	0.51664	28.91
40 %	18.07	0.00012157	3.552E+12	0.55902	17.88
50 %	25.64	0.00013324	7.282E+11	0.49494	25.45

of the coating and a decrease in its anti-corrosion performance. In the phase angle diagram, each coating has only one time constant, the peak intensity has not changed significantly, and the peak position moves in the direction of high frequency, which also indicates that the barrier performance of the coating has been reduced to varying degrees. In order to better explain the corrosion behavior of coatings with different contents soaked in NaCl solution for the same time, the Zview commercial software was used to fit the Nyquist spectrum, and the equivalent circuit diagram was obtained as shown in Fig. 6. In this equivalent circuit diagram (Fig. 4), Rs represents solution resistance, Rp represents passivating film resistance, Rct represents charge transfer resistance at the interface between coating and substrate, CPE-c represents coating capacitance, CPE-ct represents the capacitance between layers of coating, respectively. The values of each parameter in the equivalent circuit diagram are shown in Table 4. Generally, the larger of the Rp, the more difficult the electrochemical reaction is to carry out. It can be seen that with the increase of content, the passivating film resistance first increases and then decreases, and the passivating film resistance is the largest at 40 % content, indicating that the corrosion resistance of 40 % coating is better than that of other content, and can effectively reduce the erosion of corrosive media on the matrix material, which is consistent with the results of the polarization curve.

In summary, the electrochemical AC impedance analysis of the coating shows that the coating has the best corrosion resistance when the pigment content is 40 %. The anti-corrosion performance of the coating increases with the increase of pigment addition, but too much pigment addition may increase the microscopic defects inside the coating, resulting in a decrease in the compactness of the coating, thus affecting the corrosion resistance of the coating.

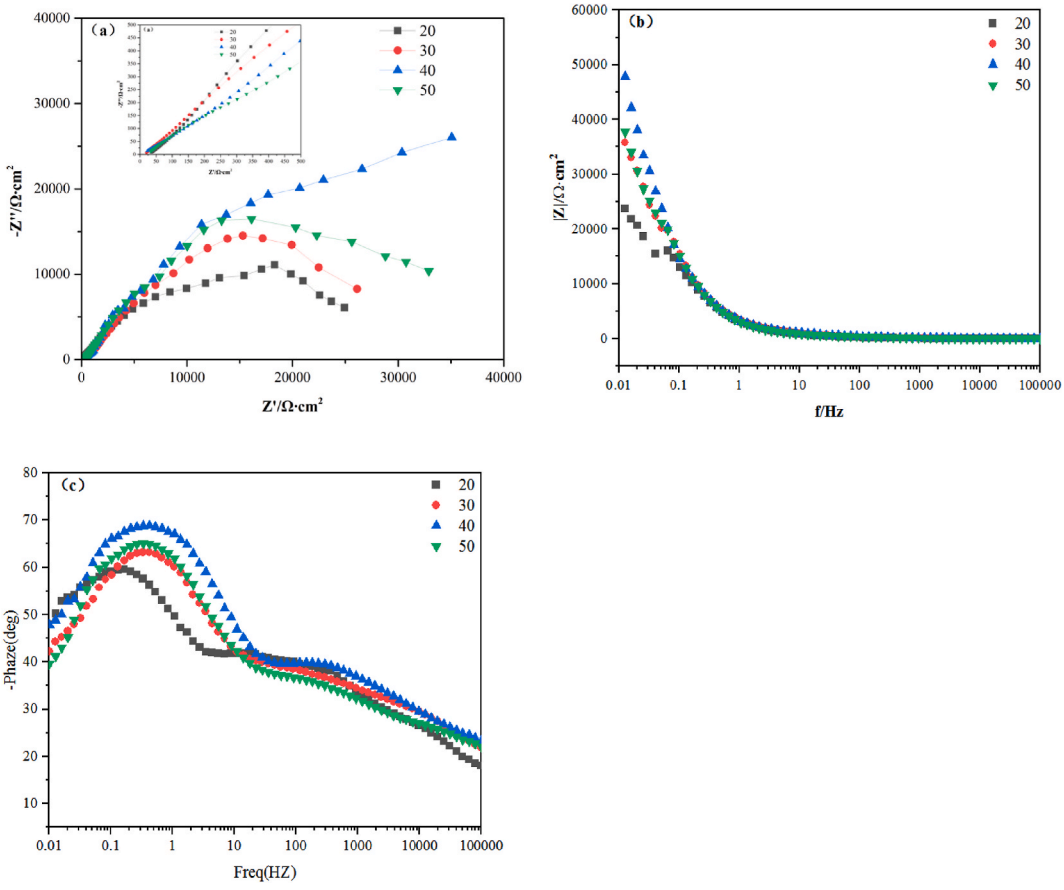

Fig. 6. (a) Nyquist plots and fitting results, (b) Bode plots and (c) Phase-frequency curves of coatings with different pigment content immersed in 3.5 % NaCl solution for 504 h.

Table 4
Fitted results for EIS curves at 504 h in 3.5 wt% NaCl.

Content	R_s/Ω	CPE-c/(S·sn1)	Rp/Ω	CPE-ct/(S·sn2)	Rct/Ω
20 %	33.82	0.00010979	1.266E+12	0.57292	33.22
30 %	13.95	0.00010238	2.522E+12	0.52899	13.74
40 %	16.69	0.00010803	4.888E+12	0.49078	16.4
50 %	33.82	0.00010979	1.266E+12	0.57292	33.22

(2) Polarization curve of coating

In order to further investigate the corrosion potential of the coatings and determine the effect of pigment content on the corrosion resistance of the coatings, four coatings with different pigment contents were subjected to potentiodynamic polarization curve testing. Each coating was immersed in 3.5 % NaCl solution for 24 h, and the polarization curves of the coatings were tested at room temperature. The measured potentiodynamic polarization curves are shown in Fig. 7. The coating remained intact during the test, and the measured potentiodynamic polarization curve could reflect the corrosion characteristics of the coating. It can be seen that the current density of each coating gradually decreases as the voltage moves forward. The measured coating polarization curve data obtained by Tafel curve extrapolation method for the corrosion potential E_{corr} and corrosion current density i_{corr} are shown in Table 5 and Fig. 8 and Fig. 9. Comparing the corrosion potential and corrosion current of the coating immersed in 3.5 % NaCl solution for 24 h, it can be found that E_{corr} is the largest and i_{corr} is the smallest for the coating with 40 % pigment content, and E_{corr} is the smallest and i_{corr} is the largest for the coating with 20 % pigment content. Therefore, the coating with 40 % pigment content has the best corrosion resistance, and the coating with 20 % pigment content has the worst corrosion resistance. When the pigment content was increased from 20 % to 30 %, the corrosion current of the coating decreased from 2.994×10^{-6} A to 9.481×10^{-7} A, reduced by about an order of magnitude. When the pigment content was increased from 30 % to 40 %, the corrosion current of the coating decreased to 3.377×10^{-7} A, but when the pigment content was increased from 40 % to 50 %, the corrosion current of the coating increased again to 6.574×10^{-7} A, which also indicated that the corrosion resistance of the coating did not keep improving with the increase of pigment content. To this end, the experimental results are consistent with the EIS test results, and the coating corrosion current density is the smallest and the coating corrosion resistance performance is the best when the pigment addition is at 40 %.

(3) Energy spectrum analysis of coatings with different pigment contents

Fig. 10 shows that Energy spectrums of (a-e) 20 %, (b-f) 30 %, (c-g) 40 % and (d-h) 50 % pigment coating after immersion corrosion in 3.5 wt% NaCl solution for 21 days, respectively. Table 6 shows the elemental content in each coating test area. It can be seen that the main components of the coatings are zinc, silicon and oxygen, etc. The silicon and oxygen elements indicate that there are chemical bonds formed by silicon and oxygen in the coatings, and the chemical bonds enhance the adhesion between the coating and the substrate, so that the coatings are firmly attached to the substrate surface. The elemental composition of the coating has more chlorine elements than that before immersion corrosion, mainly from the corrosion medium NaCl solution, chlorine ion was adsorbed by the hydrotalcite on the surface of zinc powder, and undergoes ion exchange reaction with MoO_4^{2-}. The iron element detected in the coating with 20 % pigment content is much higher than of the coating with other pigment content, which indicates that the corrosion medium has penetrated into the substrate and the coating substrate has been corroded. The barrier performance of the coating with other

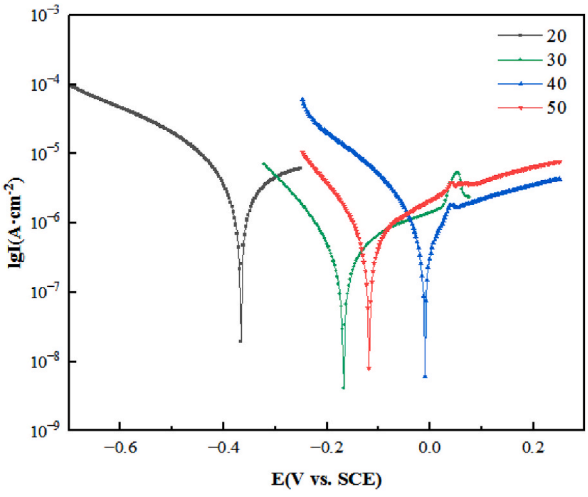

Fig. 7. Polarization curves of coatings with different pigment contents immersed in 3.5 % NaCl solution for 24 h

Table 5
Electrochemical corrosion parameters of coatings with different pigment contents.

Coating pigment content (%)	Corrosive potential E_{corr} (V vs. SCE)	Corrosive current density i_{corr} (A-cm)$^{-2}$
20	−0.364	2.994×10^{-6}
30	−0.168	9.481×10^{-7}
40	−0.017	3.377×10^{-7}
50	−0.116	6.574×10^{-7}

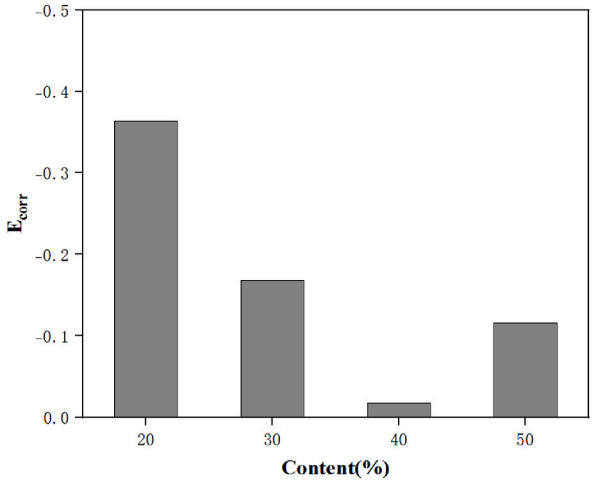

Fig. 8. Corrosion potential of coatings with different pigment content.

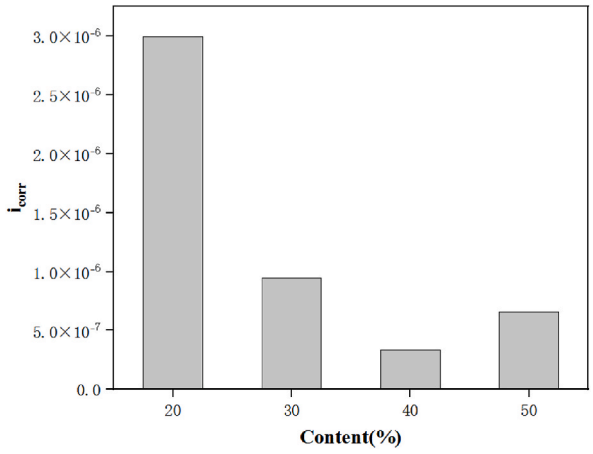

Fig. 9. Corrosion current density of coatings with different pigment content.

pigment content is better, and there are few corrosive media that diffuse to the substrate, and the substrate has not yet started to corrode. Meanwhile, the coatings with a pigment content of 40 % detected the lowest elemental chlorine content, indicating the strongest corrosion resistance.

4. Conclusion

In order to improve the active protection performance of the inorganic zinc-rich coating. The KH560 modified Mo/LDH flake zinc powder samples were synthesized in situ on the surface of flake zinc powder by hydrothermal synthesis and ion exchange method. Based on the analytical characterization results of XRD and FT-IR, it can be concluded that the synthesized samples have typical characteristic diffraction peaks of hydrotalcite and good crystal structure, showing a relatively significant hydrotalcite pillared layered structure. When the pigment content is 40 % of the base material, the coating has a smooth and uniform appearance with a metallic luster, good bonding condition with the substrate and strong adhesion. The test results of electrochemical impedance and polarization

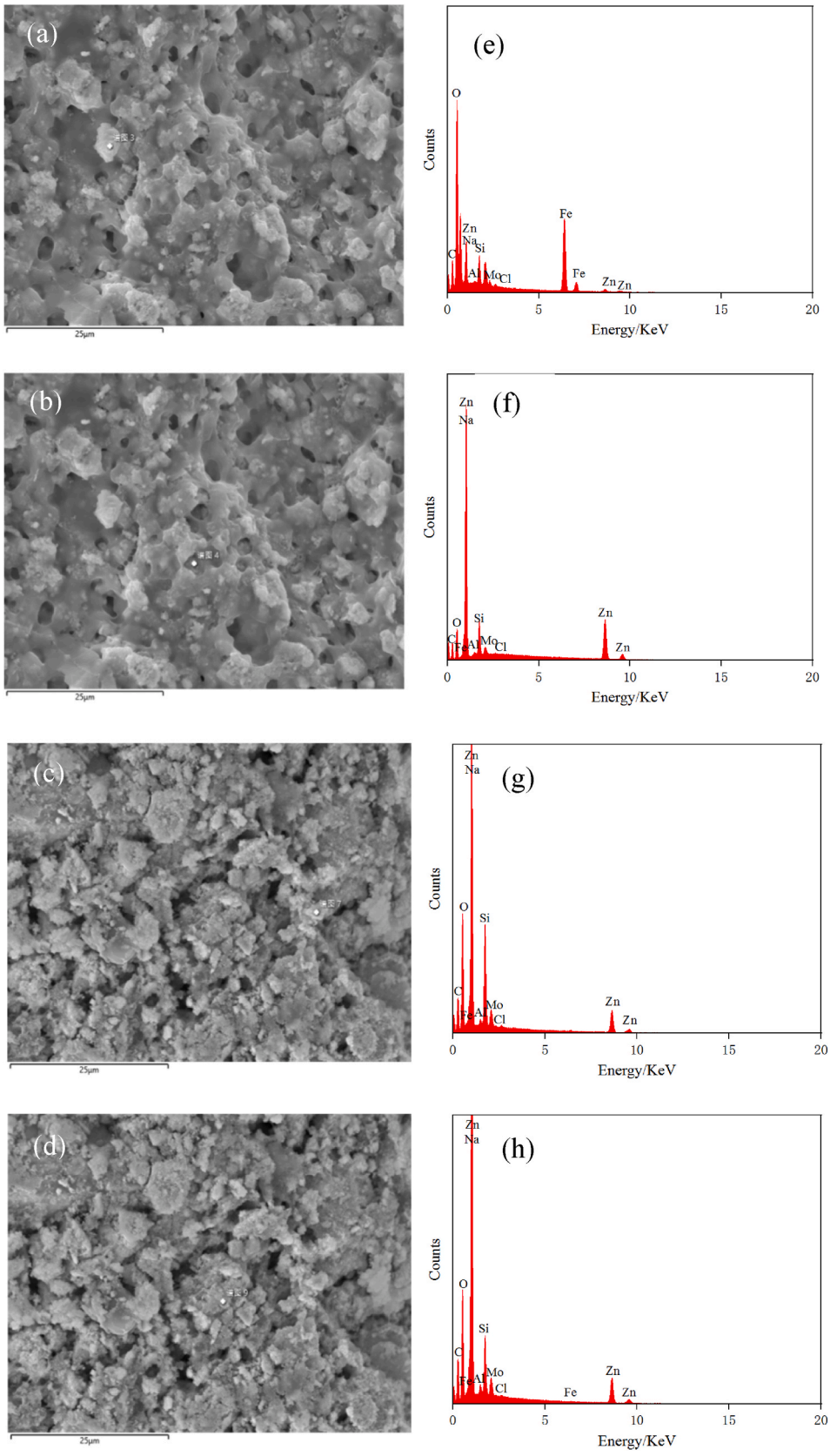

(caption on next page)

Fig. 10. Energy spectrums of (a–e) 20 %, (b–f) 30 %, (c–g) 40 % and (d–h) 50 % pigment coating after immersion corrosion in 3.5 wt% NaCl solution for 21 days.

Table 6
Comparison of elemental content in each coating test area.

Element	20 %		30 %		40 %		50 %	
	Wt%	At%	Wt%	At%	Wt%	At%	Wt%	At%
O	29.57	44.85	11.10	17.17	22.48	30.32	18.33	25.63
Si	2.52	2.18	5.56	4.90	8.79	6.75	4.47	3.56
Cl	0.31	0.21	0.18	0.13	0.11	0.07	0.16	0.10
Zn	9.93	3.69	51.92	19.65	36.78	12.14	43.66	14.94
Fe	40.19	17.46	0.21	0.09	0.10	0.04	0.13	0.05
Mo	1.11	0.28	0.00	0.00	0.00	0.00	0.01	0.00

curve of the coating show that its Nyquist curvature radius and modulus value are the largest, the maximum corrosion potential is −0.017V, and the minimum corrosion current density is 3.377 × 10-7A-cm^{-2}, indicating that the coating with a pigment content of 40 % has the best corrosion resistance. The results can be applied to metal protection in the fields of cross-sea bridges, natural gas and oil pipelines, and have good application prospects.

Data availability statement

All data generated or analysed during this study are included in this published article.

CRediT authorship contribution statement

Shuangxi Zhou: Data curation, Conceptualization. **Weijie Li:** Writing – original draft, Formal analysis, Data curation. **Jianxin Li:** Investigation. **Ruguang Li:** Writing – review & editing, Supervision.

Declaration of competing interest

The authors declare the following financial interests/personal relationships which may be considered as potential competing interests:Zhou Shuangxi reports financial support was provided by National Natural Science Foundation of China. If there are other authors, they declare that they have no known competing financial interests or personal relationships that could have appeared to influence the work reported in this paper.

Acknowledgments

Funding by the National Natural Science Foundation of China, 51968022; Academic and Technical Leader of Major disciplines in Jiangxi Province, No. 20213BCJL22039; Guangdong Province Key Construction Discipline Research Ability Improvement Project (2022ZDJS095).

References

[1] S.X. Zhou, W.J. Li, Z.Y. Ai, et al., Research Progress of inorganic silicate zinc rich anticorrosive coatings, J]. Materials Protection 55 (8) (2022) 1–7.
[2] G. Sun, H. Zhou, X. Cao, et al., Self-assembled Multilayer structure and enhanced Thermochromic performance of Spinodally Decomposed TiO_2-VO_2 Thin film, ACS Appl. Mater. Interfaces (2016) 7054–7059.
[3] M.F. Montemor, Functional and smart coatings for corrosion protection: a review of recent advances, Surf. Coating. Technol. 258 (2014) 17–37.
[4] M. Plawecka, D. Snihirova, B. Martins, et al., Self healing ability of inhibitor-containing nanocapsules loaded in epoxy coatings applied on aluminium 5083 and galvanneal substrates, Electrochim. Acta 140 (2014) 282–293.
[5] I.B. Recalde, N. Estebanez, L. Frances-Soriano, et al., Upconversion nanoparticles with a strong acid-resistant capping, Nanoscale 8 (14) (2016) 7588–7594.
[6] R. Padash, M. Rahimi-Nasrabadi, A. Shokuhi Rad, et al., A theoretical study of two novel Schiff bases as inhibitors of carbon steel corrosion in acidic medium, Appl. Phys. A 125 (2) (2019) 78.
[7] D.G. Shchukin, H. Möhwald, Surface-engineered nanocontainers for entrapment of corrosion inhibitors, Adv. Funct. Mater. 17 (9) (2010) 1451–1458.
[8] E.V. Skorb, D.G. Shchukin, H. Mhwald, et al., Photocatalytically-active and photocontrollable coatings based on titania-loaded hybrid sol–gel films, J. Mater. Chem. 19 (2009) 4931–4937.
[9] D. Snihirova, S.V. Lamaka, M. Taryba, et al., Hydroxyapatite microparticles as feedback-active reservoirs of corrosion inhibitors, ACS Appl. Mater. Interfaces 2 (11) (2010) 3011.
[10] G.M. Liu, X.S. Zhou, Y.Y. Wang, et al., Preparation of modified hydrotalcite and its effect on properties of epoxy zinc rich paint, Surf. Technol. 46 (3) (2017) 223–228.
[11] X. Yu, Z.D. Yu, L.H. Cheng, et al., Corrosion resistance of hydrotalcite nanocontainers loaded with zinc/molybdate corrosion inhibitors, Electroplating & Finishing 32 (1) (2013) 72–75.
[12] L. Mohapatra, K. Parida, M. Satpathy, Molybdate/tungstate intercalated oxo-bridged Zn/Y LDH for solar light induced photodegradation of organic pollutants, J. Phys. Chem. C 116 (24) (2012) 13063–13070.

[13] L. Li, S.J. Liu, B.S. Li, et al., Preparation and characterization of zinc aluminum hydrotalcite intercalated with organic ultraviolet absorbent, Chin. J. Inorg. Chem. 23 (3) (2007) 407–414.
[14] D. Carriazo, C. Martin, V. Rives, An FT-IR study of the adsorption of isopropanol on calcined layered double hydroxides containing isopolymolybdate, Catal. Today 126 (1–2) (2007) 153–161.
[15] J.M. Sanchez-Amaya, R.M. Osuna, M. Bethencourt, et al., Monitoring the degradation of a high solids epoxy coating by means of EIS and EN, Prog. Org. Coating 60 (3) (2007) 248–254.